Residues within a lipid-associated segment of the PECAM-1 cytoplasmic domain are susceptible to inducible, sequential phosphorylation

*Cathy Paddock,[1] *Betsy L. Lytle,[2] Francis C. Peterson,[2] Trudy Holyst,[1] Peter J. Newman,[1,3-4] Brian F. Volkman,[2] and Debra K. Newman[1,3,5]

[1]Blood Research Institute, BloodCenter of Wisconsin and Departments of [2]Biochemistry, [3]Pharmacology and Toxicology, [4]Cell Biology, Neurobiology and Anatomy, and [5]Microbiology and Molecular Genetics, Medical College of Wisconsin, Milwaukee, WI

Immunoreceptor tyrosine-based inhibitory motif (ITIM)–containing receptors inhibit cellular responsiveness to immunoreceptor tyrosine-based activation motif (ITAM)–linked receptors. Although tyrosine phosphorylation is central to the initiation of both inhibitory ITIM and stimulatory ITAM signaling, the events that regulate receptor phosphorylation are incompletely understood. Previous studies have shown that ITAM tyrosines engage in structure-inducing interactions with the plasma membrane that must be relieved for phosphorylation to occur. Whether ITIM phosphorylation is similarly regulated and the mechanisms responsible for release from plasma membrane interactions to enable phosphorylation, however, have not been defined. PECAM-1 is a dual ITIM-containing receptor that inhibits ITAM-dependent responses in hematopoietic cells. We found that the PECAM-1 cytoplasmic domain is unstructured in an aqueous environment but adopts an α-helical conformation within a localized region on interaction with lipid vesicles that mimic the plasma membrane. The lipid-interacting segment contains the C-terminal ITIM tyrosine and a serine residue that undergo activation-dependent phosphorylation. The N-terminal ITIM is excluded from the lipid-interacting segment, and its phosphorylation is secondary to phosphorylation of the membrane-interacting C-terminal ITIM. On the basis of these findings, we propose a novel model for regulation of inhibitory signaling by ITIM-containing receptors that relies on reversible plasma membrane interactions and sequential ITIM phosphorylation. (*Blood*. 2011;117(22):6012-6023)

Introduction

Immunoreceptor tyrosine-based inhibitory motif (ITIM)–containing receptors oppose cellular activation by receptors that are coupled to immunoreceptor tyrosine based-activation motif (ITAM)–containing subunits.[1] The inhibitory function of ITIM-containing receptors depends on Src homology (SH) 2 domain–dependent binding of tyrosine or inositol phosphatases to phosphorylated ITIMs within the cytoplasmic domain and subsequent dephosphorylation of signal transduction pathway components that are required for ITAM-dependent cellular activation.[1] Src family kinases initiate signaling by both ITIM- and ITAM-containing receptors; however, the mechanisms that control access of ITIM or ITAM sequences to active Src family kinases are not well understood. Recent studies have revealed that the ITAMs of T-cell receptor–associated signaling subunits, which are intrinsically unstructured in an aqueous environment, exhibit increased α-helical content and decreased phosphorylation on interaction with detergent or phospholipid vesicles that mimic the plasma membrane.[2-4] These findings suggested that signal transduction by ITAM-containing receptors is regulated by reversible membrane association. The extent to which this principle applies to ITIM-containing receptors has not been determined.

The ITIM-containing receptor family encompasses a large number of different Ig-domain–containing and C-type lectin receptors that are expressed on an array of cells of hematopoietic origin.[1] Platelet Endothelial Cell Adhesion Molecule-1 (PECAM-1) is a member of the Ig-ITIM subfamily of ITIM-containing receptors[5] that is expressed on all endothelial cells and on most hematopoietic cells, including platelets, mast cells, lymphocytes, and monocytes.[6] PECAM-1 is a 130-kDa type I transmembrane glycoprotein that contains 6 extracellular Ig homology domains, a single-pass transmembrane region, and a long cytoplasmic domain that contains 2 ITIMs surrounding tyrosine (Y) residues that are found at positions 663 and 686 within the mature form of human PECAM-1, the phosphorylation of which supports recruitment and activation of Src homology 2 domain–containing protein tyrosine phosphatases, including SHP-2 and, to a lesser extent, SHP-1.[7] Formation of PECAM-1/SHP-2 complexes is associated with inhibition of platelet, mast cell, and lymphocyte activation via ITAM-coupled receptors.[7] As with other ITIM-containing receptors, Src family kinases are involved in PECAM-1 tyrosine phosphorylation[7]; however, the mechanisms that control phosphorylation of the PECAM-1 ITIMs are not known.

In the present study, we determined the structure of the ITIM-containing PECAM-1 cytoplasmic domain, in the presence and absence of detergent micelles to mimic the plasma membrane. We found that the PECAM-1 cytoplasmic domain was intrinsically unstructured in aqueous solution but that a localized region of it adopted α-helical conformation on interaction with a plasma membrane mimetic. The membrane-interacting portion of the PECAM-1 cytoplasmic domain encompassed the C-terminal ITIM,

Submitted November 9, 2010; accepted March 21, 2011. Prepublished online as *Blood* First Edition paper, April 4, 2011; DOI 10.1182/blood-2010-11-317867.

*C.P. and B.L.L., representing the laboratories of D.K.N. and B.F.V., contributed equally to this work.

The online version of this article contains a data supplement.

The publication costs of this article were defrayed in part by page charge payment. Therefore, and solely to indicate this fact, this article is hereby marked "advertisement" in accordance with 18 USC section 1734.

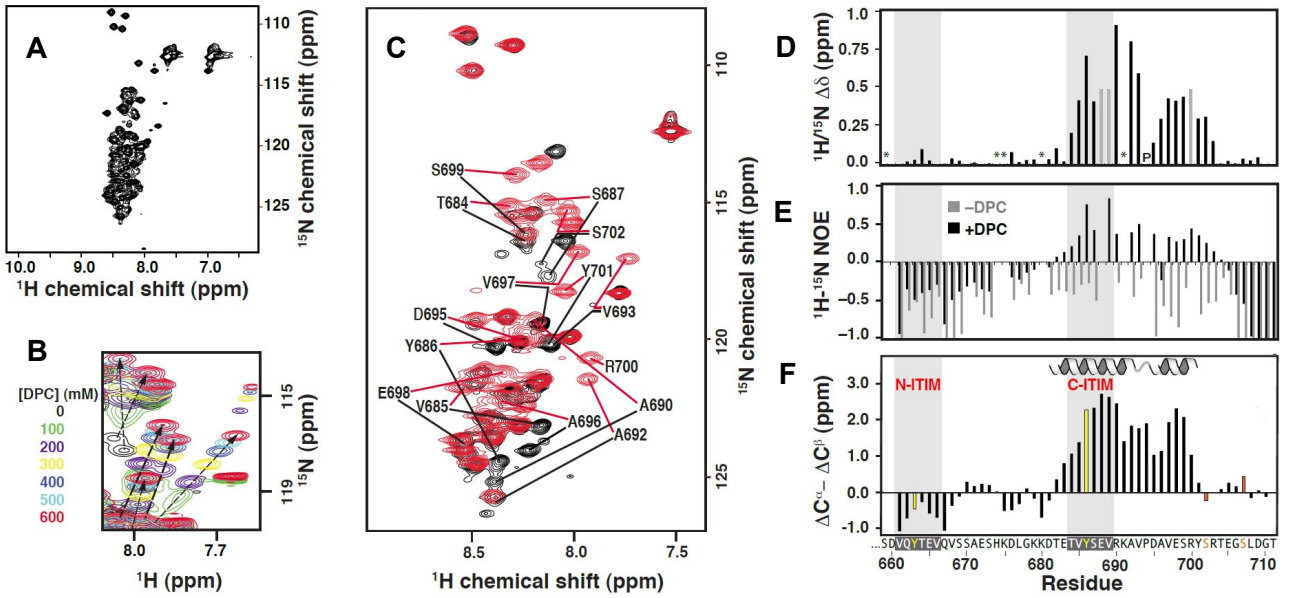

Figure 1. A segment spanning residues 684-702 of the PECAM-1 cytoplasmic domain interacts with DPC micelles. (A) The HSQC spectrum of ^{15}N–labeled PECAM$_{594\text{-}711}$, generated as described in supplemental Figure 1, reveals its intrinsically unstructured nature. (B) HSQC spectra of ^{15}N–labeled PECAM$_{594\text{-}711}$ at DPC concentrations ranging from 0-600mM. Arrows highlight residues that shift and are presumed to participate in DPC binding. (C) PECAM$_{659\text{-}711}$ HSQC signals in the absence (black) and presence (red) of DPC micelles exhibiting ^{1}H/^{15}N chemical shift differences greater than 0.2 ppm are labeled with their single-letter amino acid code and position within full-length human PECAM-1. (D) Plot of the combined ^{1}H/^{15}N chemical shift difference for residues of PECAM$_{659\text{-}711}$ in the absence versus presence of 600mM DPC. Gray bars indicate residues for which backbone resonances were detected in one but not the other sample (and thus, no shift difference could be calculated). Proline 694 is marked with "P," and residues where it was not possible to make assignments because of missing or overlapping cross peaks are indicated with asterisks. (E) Heteronuclear ^{1}H-^{15}N NOE values in the absence (gray) and presence (black) of DPC indicate that residues perturbed by micelles also become more ordered. Residues for which the hetNOE value could not be determined have a value of 0. (F) Three-residue averaged secondary shifts, where $(\Delta C^{\alpha} - \Delta C^{\beta})_i = 1/3(\Delta C^{\alpha}_{i-1} + \Delta C^{\alpha}_{i} + \Delta C^{\alpha}_{i+1} - \Delta C^{\beta}_{i-1} - \Delta C^{\beta}_{i} - \Delta C^{\beta}_{i+1})$, versus residue sequence numbers *i*.[18] Each ΔC^{α} and ΔC^{β} in the equation is the deviation between the experimentally observed and random coil chemical shift value of $^{13}C^{\alpha}$ and $^{13}C^{\beta}$, respectively.[19,20] Characteristic positive $(\Delta C^{\alpha} - \Delta C^{\beta})$ values predict a helix spanning T_{682}-Y_{701}.

which became preferentially phosphorylated relative to the non–membrane-interacting N-terminal ITIM, as well as a serine residue that was susceptible to inducible phosphorylation. On the basis of these results, we conclude that plasma membrane interactions control access of cytoplasmic ITIM and serine residues to the kinases that phosphorylate them.

Methods

NMR spectroscopy

Generation of the recombinant proteins that encompassed the entire (PECAM$_{594\text{-}711}$) or the C-terminal half (PECAM$_{659\text{-}711}$) of the PECAM-1 cytoplasmic domain is described in supplemental Methods (available on the *Blood* Web site; see the Supplemental Materials link at the top of the online article). A two-dimensional ^{15}N,^{1}H heteronuclear single quantum coherence (HSQC) titration experiment was performed with a sample that contained ~ 600μM ^{15}N-labeled PECAM$_{594\text{-}711}$ in nuclear magnetic resonance (NMR) buffer that contained 90% H_2O/10% D_2O. For dodecylphosphocholine (DPC) dose-response studies, 600mM DPC was added after the first spectrum was collected, and buffer that contained 600μM PECAM$_{594\text{-}711}$ was added for each subsequent titration point. Paramagnetic broadening was measured by acquiring 2-dimensional ^{1}H-^{13}C HSQC spectra on PECAM$_{659\text{-}711}$ with 600 mM DPC in the presence and absence of 0.5 mM $MnCl_2$. Three-dimensional (3D) heteronuclear backbone experiments and heteronuclear ^{15}N-^{1}H nuclear Overhauser effect (hetNOE) experiments[8] were performed as described previously[9] with samples that contained 1.25mM ^{13}C/^{15}N-labeled PECAM$_{594\text{-}711}$ or PECAM$_{659\text{-}711}$ with or without 600mM DPC in the same buffer. NMR data were acquired at 25°C on a Bruker 500-MHz spectrometer equipped with a triple-resonance CryoProbe and processed with NMRPipe software.[10] Initial ^{1}H, ^{15}N, and ^{13}C resonance assignments for PECAM$_{594\text{-}711}$ (+DPC) were obtained from the PINE-NMR server[11] (version 1.0; http://miranda.nmrfam.wisc.edu/PINE/), with peak lists from 3D HNCO, HN(CA)CO, HNCA, HN(CO)CA, HNCACB, and CCONH spectra. Tentative assignments were manually inspected, edited, and completed with XEASY[12] for 85% of the residues from 629-711. Assignments were transferred to the PECAM$_{594\text{-}711}$ (−DPC) spectra and adjusted manually with the DPC titration data for resonances that had shifted. Backbone assignments were subsequently verified and completed for 90% of the residues in PECAM$_{659\text{-}711}$ in the presence and absence of DPC. The combined chemical shift difference for each residue was calculated as $[(0.154*\delta_N)^2 + (\delta_H)^2]^{1/2}$, where δ_N and δ_H are the ^{15}N and $^{1}H^{N}$ chemical shift differences (parts per million [ppm]), respectively, between the two conditions.[13]

Peptide synthesis

Peptides encompassing residues 684-711 of PECAM-1 were synthesized with standard Fmoc protocols on an ABI 433 instrument. Phosphorylated serine and tyrosine (pS_{702} and pY_{686}) residues were coupled as protected amino acids. The peptide resin was cleaved with 92.5% trifluoroacetic acid (TFA), 2.5% ethanedithiol, 2.5% Trisisopropylsilane, and 2.5% H_20 and precipitated in cold ethyl ether. Peptides were purified to > 90% by reversed-phase HPLC with a Phenomenex Proteo C12 column and a 0.1% TFA/acetonitrile gradient. The mass of the final product was verified by matrix-assisted laser desorption/ionization time-of-flight (MALDI-TOF) mass spectrometry.

Structure calculations of PECAM$_{659\text{-}711}$

Side-chain assignments for PECAM$_{659\text{-}711}$ in the presence of DPC were completed manually from 3D HBHACONH, HCCH-TOCSY, ^{13}C-edited NOESY-HSQC spectra, and ^{13}C(aromatic)-edited NOESY-HSQC spectra. Backbone Φ and Ψ dihedral angle constraints were generated from secondary shifts of the $^{1}H^{\alpha}$, $^{13}C^{\alpha}$, $^{13}C^{\beta}$, $^{13}C'$, and ^{15}N nuclei shifts with TALOS+.[14] Distance constraints were obtained from 3D ^{15}N-edited NOESY-HSQC and ^{13}C-edited NOESY-HSQC spectra (t_{mix} = 80 ms). Structure calculations were performed with the torsion angle dynamics

Table 1. Statistics for the 20 PECAM-1$_{677\text{-}711}$ conformers

Experimental constraints, n	
Distance constraints	
Long	0
Medium [$1 < (i-j) \leq 5$]	41
Sequential [$(i-j) = 1$]	42
Intraresidue [$i = j$]	81
Total	164
Dihedral angle constraints (ϕ and ψ)	33
Average atomic RMSD to the mean structure, Å	
Residues 682-701	
Backbone (C^{α}, C′, N)	0.57 ± 0.24
Heavy atoms	1.12 ± 0.25
Deviations from idealized covalent geometry	
Bond lengths, RMSD, Å	0.013
Torsion angle violations, RMSD, degrees	1.2
Constraint violations	
NOE distance, No. > 0.5 Å*	0.0 ± 0
NOE distance, RMSD, Å	0.028 ± 0.004
Torsion-angle violations,† No. > 5	0.0 ± 0
Torsion-angle violations, RMSD, degrees	0.404 ± 0.117
WHAT_CHECK quality indicators	
Z-score	−2.42 ± 0.46
RMS Z-score	
Bond lengths	0.67 ± 0.04
Bond angles	0.66 ± 0.03
Bumps	0 ± 0
Lennard-Jones energy,‡ kJ mol^{-1}	−339 ± 42
Ramachandran statistics, % of all residues	
Most favored	83.12 ± 4.61
Additionally allowed	13.44 ± 4.17
Generously allowed	2.74 ± 2.87
Disallowed	0.68 ± 1.80

RMSD indicates root mean square deviation.
*The largest NOE violation in the ensemble of structures was 0.30 Å.
†The largest torsion-angle violation in the ensemble of structures was 2.5°.
‡Nonbonded energy was calculated in XPLOR-NIH.

program CYANA.[15] The final structure calculation included residues 677-711 only, with most of the unstructured N-terminal region omitted. Of the 100 CYANA structures calculated, the 20 conformers with the lowest target function were subjected to a molecular dynamics protocol in explicit solvent[16] with XPLOR-NIH.[17]

The atomic coordinates (PDB ID 2KY5) are deposited in the Protein Data Bank (http://www.rcsb.org/), and the NOE distance constraints and dihedral angle constraints (BMRB ID 16935) are deposited at the Biological Magnetic Resonance Bank (http://www.bmrb.wisc.edu/).

Circular dichroism spectroscopy

Small unilamellar vesicles were prepared with 1,2-dimyristoyl-sn-glycero-3-[phospho-L-serine] (DMPS) and/or 1,2-dimyristoyl-sn-glycero-3-phosphocholine (DMPC; Avanti Polar Lipids), which was dried to a film and lyophilized overnight to remove solvent, resuspended in 20mM Na_2HPO_4 (pH 7), and sonicated at high intensity in a cup horn sonicator (Qsonica). Circular dichroism (CD) measurements (5 scans/measurement) were made with a Jasco J-710 spectropolarimeter at room temperature over a 190- to 250-nm range with a bandwidth of 1 nm and a scanning rate of 50 nm/min. For the data shown in Figure 8A, each sample contained 100μM peptide and a 6mM final concentration of small unilamellar vesicles composed of 100% DMPC, 75% DMPC/25% DMPS, 50% DMPC/50% DMPS, or 100% DMPS. For the data shown in Figures 8B-C, each sample contained 100μM peptide and small unilamellar vesicles composed of 100% DMPS at a final concentration of 0, 1.5, 3, or 6mM. Spectra were corrected for buffer and vesicle effects by subtracting scans obtained with the appropriate concentration of vesicle only. Linear regression analysis was performed with GraphPad Prism 5 software.

In vitro tyrosine phosphorylation of the PECAM-1 cytoplasmic domain and purification of phosphorylated and unphosphorylated species

PECAM$_{594\text{-}711}$Y$_{636,701}$F was incubated with Src (BIOMOL), Fyn (BIOMOL), or Fer (Cell Signaling) in buffer that contained 0.25mM ATP/1mM EGTA/10mM $MgCl_2$/0.01% Brij-35/0.25mM Na_3VO_4 overnight at 30°C. We were unable to perform in vitro kinase assays in the presence of DPC because neither Src nor Fer family kinases were active in the presence of DPC (data not shown). Phosphorylated and unphosphorylated species were separated on a Mono Q column in 10mM BIS-TRIS Propane (pH 6.2) that contained 1mM DTT with a gradient of 20-250mM NaCl over 50 minutes at a flow rate of 0.5 mL/min on an Akta FPLC system (GE Healthcare).

Mass spectrometric analysis of PECAM-1$_{594\text{-}711}$ tryptic digests

Peak protein-containing fractions obtained from Mono Q column chromatography were diluted in 0.1% TFA (1:1), desalted, eluted from P10 C18 Ziptips (Millipore) into 80% acetonitrile/0.1% TFA, and dried in a SpeedVac (Thermo Scientific). Samples were resuspended in 25mM NH_4CO_3 (pH 8) and digested with trypsin (62.5 ng) for 1 hour at 37°C. Tryptic digests were eluted from P10 C18 Ziptips with 80% acetonitrile/0.1% TFA, spotted with DHB (2,5-dihydroxybenzoic acid) or CHCA (α-cyano-4-hydroxycinnamic acid) matrix, and dried under vacuum. MALDI-TOF data were acquired with an ABI Voyager-DE Pro mass spectrometer in positive ion, linear mode. Data were analyzed with Data Explorer (Applied Biosystems) and calibrated on known PECAM-1 fragments present in every sample. Observed masses were compared with expected masses generated from *in silico* digestion of PECAM$_{594\text{-}711}$Y$_{636,701}$F with Protein Prospector (University of California at San Francisco Mass Spectrometry Facility), which required 5 missed cleavages to ensure the presence of both ITIMs in a single peptide.

Identification of phosphorylated serine residues with mutant forms of recombinant PECAM-1

Human embryonic kidney (HEK) 293T cells were transiently transfected with PECAM-1–encoding plasmids with Superfect (Qiagen), washed with serum- and phosphate-free DMEM, and exposed to ^{32}P-orthophosphate (0.2 mCi/mL) with or without 1μM okadaic acid (OA) for 4 hours. Cells were lysed in buffer that contained 20mM Tris/150mM NaCl/1% Triton X-100/1mM EDTA/10mM NaF/20mM β-glycerophosphate, serine phosphatase inhibitors (Calbiochem), and complete protease inhibitor cocktail tablets (Roche). PECAM-1 was immunoprecipitated from precleared cell lysates with PECAM-1.3, and immunoprecipitates were resolved by SDS-PAGE. Parallel gels were fixed, dried, and used to expose X-OMAT film with a Lightning Plus LK screen overnight at −80°C or subjected to Western blot analysis with rabbit polyclonal anti-human PECAM-1 antibodies to quantify PECAM-1 levels.

Generation and characterization of PECAM-1 pS$_{702}$-, pS$_{707}$-, and pY$_{686}$-specific polyclonal antibodies

Affinity-purified rabbit antibodies specific for human PECAM-1 phosphorylated on tyrosine 686 (anti-pY$_{686}$), serine 702 (anti-pS$_{702}$), or serine 707 (anti-pS$_{707}$) were commissioned from BioSource International with the following used as immunogens: acetyl-DTETVpY$_{686}$SEVRKA(C)-amide, acetyl-(C)VESRYpS$_{702}$RTEGS-amide, and acetyl-SRTEGpS$_{707}$LDGT(C)-amide phosphopeptides, respectively. To verify specificity, HEK 293T cells transfected with plasmids encoding wild-type (WT) or mutant forms of PECAM-1 were cultured in the presence and absence of OA (to characterize phosphoserine-specific antibodies) or pervanadate (to characterize pY$_{686}$-specific antibodies), lysed, and subjected to PECAM-1 immunoprecipitation and Western blot analysis as described above.

Assessment of PECAM-1 pY$_{686}$, pS$_{702}$, and pS$_{707}$ levels in resting, activated, and aggregated platelets

Washed human platelets in 1mM $CaCl_2$/1mM $MgCl_2$/0.3 mg/mL fibrinogen were left unstimulated (resting) or were stimulated, under stirring conditions (1000 rpm), for 2 minutes with thrombin receptor activating peptide

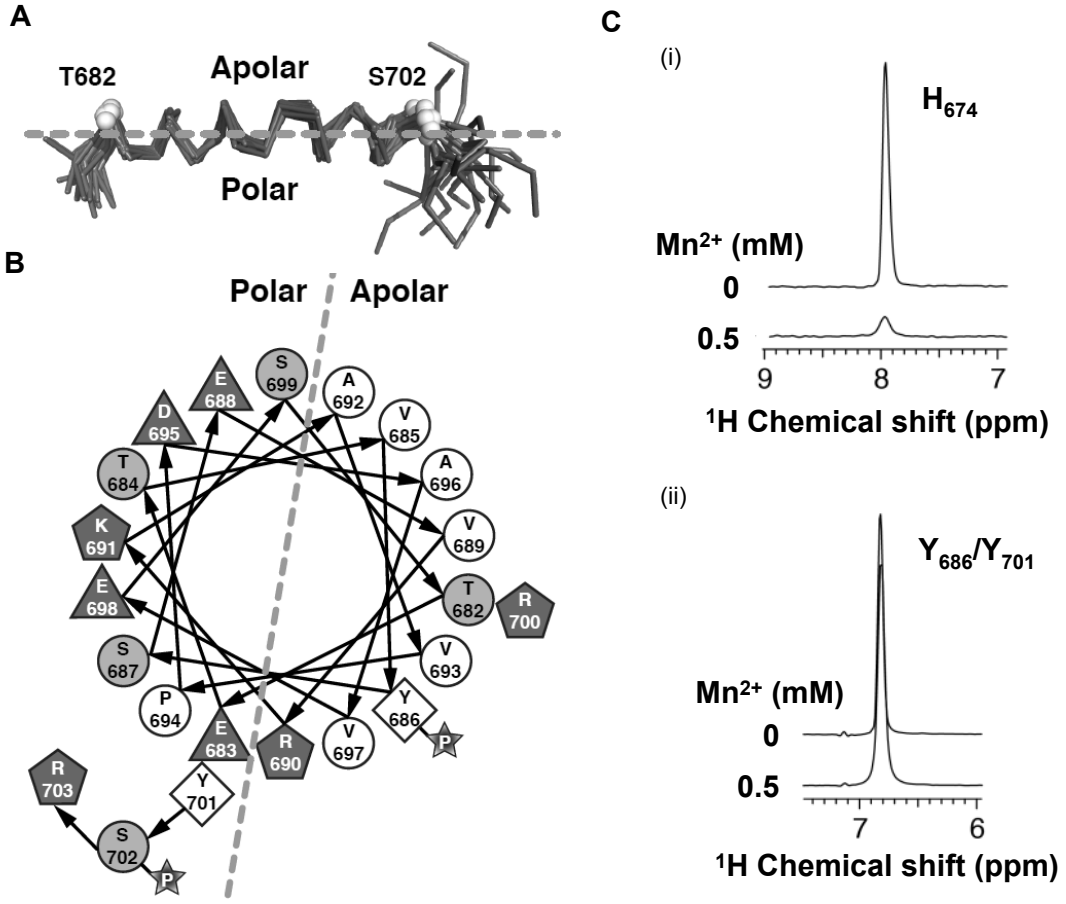

Figure 2. Structure of $PECAM_{659-711}$ in the presence of DPC. (A) Cα backbone trace representation of the NMR ensemble of 20 structures superimposed over residues 682-701. Unstructured residues 659-679 and 706-711 are not shown for clarity. (B) Helical wheel diagram illustrating the amphipathic nature of the DPC-stabilized structure. Hydrophobic (white circles), polar (gray circles), and charged (gray polygons) residues are labeled by amino acid type and number. (C) One-dimensional ^{1}H slices from aromatic ^{1}H-^{13}C HSQC spectra of $PECAM_{659-711}$ in the presence of DPC show that addition of 0.5mM Mn^{2+} induces broadening of the resonance of the histidine (H_{674}) side chain, which is located outside the membrane-interacting region (i), but not of the tyrosine (Y_{686}/Y_{701}) side chains, which are located within the membrane-interacting region (ii).

(7μM) in the presence (activated) or absence (aggregated) of 2mM RGD and 5mM EDTA. Platelets were lysed (1:1) in 100mM Tris/300mM NaCl/2% Triton X-100/0.2% SDS/2% sodium deoxycholate/2mM EDTA/20mM NaF/40mM β-glycerophosphate with tyrosine and serine phosphatase inhibitors (Calbiochem) and protease inhibitors. Lysates were subjected to PECAM-1 immunoprecipitation and Western blot analysis as described above. Research involving human subjects was approved by the BloodCenter of Wisconsin Institutional Review Board, and all human participants gave written informed consent in accordance with the Declaration of Helsinki.

Results

Structure of the PECAM-1 cytoplasmic domain in the presence and absence of DPC micelles

We used an NMR approach to investigate the structural properties of the PECAM-1 cytoplasmic domain. The 2-dimensional ^{1}H-^{15}N HSQC spectrum of $PECAM\text{-}1_{594-711}$ in aqueous solution displayed ~ 89 backbone amide resonances of the 112 expected, but with a very narrow spread of resonance frequencies in both the ^{15}N and ^{1}H dimensions (Figure 1A). This pattern is characteristic of either unfolded or globally dynamic proteins.[21] On the basis of these findings, we conclude that the PECAM-1 cytoplasmic domain is intrinsically unstructured in aqueous solution.

Previous studies have reported that a segment of the ITAM-containing T-cell receptor ζ-chain cytoplasmic domain is also unstructured in an aqueous environment but adopts an α-helical structure on interaction with negatively charged phospholipids.[2-4,22] To determine whether the ITIM-containing PECAM-1 cytoplasmic domain behaves similarly, NMR spectroscopy was used to detect interactions between $PECAM_{594-711}$ and DPC micelles, which are used in NMR studies as a membrane mimetic model system.[23,24] As shown in Figure 1B, addition of DPC to $PECAM_{594-711}$ in 100-mM increments up to 600mM (the solubility limit under the experimental conditions) consistently shifted the HSQC signals for at least 16 residues toward lower ^{15}N chemical shift values. Upfield ^{15}N chemical shift changes previously have been correlated with a micelle-induced conformational change from random coil to α-helix on interaction.[25,26] To identify the residues involved in DPC binding, we assigned backbone ^{15}N, $^{1}H^{N}$, and $^{13}C'$ resonances, as well as $^{13}C^{\alpha}$ and $^{13}C^{\beta}$ resonances, for approximately 80% of the residues from N_{629}-T_{711} of $PECAM_{594-711}$ in the absence and presence of 600mM DPC. Backbone $^{1}H/^{15}N$ chemical shift perturbations clustered in the segment from T_{682} to S_{702}, which indicates that this is the region within $PECAM_{594-711}$ that interacts with DPC micelles (data not shown). To confirm and complete the resonance assignments, spectra were obtained with the C-terminal portion of the cytoplasmic domain ($PECAM_{659-711}$) wherein the amount of resonance overlap decreased significantly (Figure 1C). Chemical shift values for $PECAM_{659-711}$ were identical to those observed for the full-length form ($PECAM_{594-711}$), which indicates that the structure and DPC interactions of the PECAM-1 cytoplasmic

domain were unaffected by truncation of the unstructured N-terminal region (supplemental Figure 2). Backbone resonances of $PECAM_{659-711}$ in the presence of DPC were assigned for all residues except S_{659}, H_{674}, K_{675}, K_{680}, and K_{691}. In the absence of DPC, the additional residues E_{688}, V_{689}, and R_{700} could not be assigned. The chemical shifts were very similar to those of the full-length PECAM-1 cytoplasmic domain ($PECAM_{594-711}$), both with and without DPC. As with $PECAM_{594-711}$, analysis of $PECAM_{659-711}$ $^{1}H/^{15}N$ chemical shifts in the presence versus absence of DPC revealed that a segment from T_{682} to S_{702} was significantly perturbed on binding to DPC micelles, which indicates that the structure and DPC interaction were unaffected by truncation of the unstructured N-terminal region (Figure 1D).

To assess changes in picosecond-nanosecond dynamics of $PECAM_{659-711}$, we measured heteronuclear ^{1}H-^{15}N NOE values in the presence and absence of DPC. As expected for a dynamically disordered protein, NOE values were exclusively negative for $PECAM_{659-711}$ in the absence of DPC. In the presence of DPC micelles, significant increases in the NOE values were observed for several residues between T_{682} and R_{703} of $PECAM_{659-711}$, which denotes an increase in local order (Figure 1E). The $^{13}C^{\alpha}$ and $^{13}C^{\beta}$ chemical shifts are highly sensitive to the presence of secondary structure, and the 3-residue averaged secondary shifts (ΔC^{α}-ΔC^{β}) computed for $PECAM_{659-711}$ in the presence of DPC were significantly positive (> 0.5 ppm) for residues E_{683}-R_{700} (Figure 1F). Consistent with our secondary shift analysis, TALOS+[14] analysis of $^{1}H^{\alpha}$, $^{13}C^{\alpha}$, $^{13}C^{\beta}$, $^{13}C'$, and ^{15}N shifts predicted that residues D_{681}-Y_{701} of $PECAM_{659-711}$ would form an α-helix in the presence of DPC (data not shown). No other regular secondary structure elements were predicted, and no secondary structures were predicted in the absence of DPC.

To confirm the predicted membrane-associated conformation, we solved the NMR structure of $PECAM_{659-711}$ in the presence of DPC. The first 18 residues were dynamically disordered and were omitted in the final structure refinement (Table 1). As predicted by our TALOS+ results, the only regular structure was a helical region that spanned residues T_{682}-Y_{701} (Figure 2A). Chemical shift and NOE data were consistent with a slight bend in the helix at V_{693}-P_{694}. The helix is amphiphilic in nature, with hydrophobic side chains that included Y_{686} of the C-terminal ITIM forming a membrane-binding surface on one face of the helix and hydrophilic side chains on the opposite face (Figure 2B). The helix is not strictly amphiphilic, however, because the basic residue, R_{700}, is found on the hydrophobic face. It is therefore likely that binding to the plasma membrane is mediated by both hydrophobic interactions with the phospholipid tails and electrostatic interactions between the basic amino acid side chains and the negatively charged phosphatidylserine and phosphatidylinositol head groups. To more directly demonstrate contact between this region of the PECAM-1 cytoplasmic domain and plasma membrane mimetics, we evaluated selective paramagnetic broadening of aromatic side-chain NMR signals. The data shown in Figure 2C reflect the lower accessibility for side chains of tyrosine residues Y_{686} and Y_{701}, which are in the membrane-associated helix, relative to that of the histidine residue (H_{674}) that is away from the helix and exposed to solvent and the paramagnetic effect of Mn^{2+}. These data provide independent evidence for membrane association of the PECAM-1 cytoplasmic domain.

Sequential phosphorylation of PECAM-1 ITIMs

Phosphorylation of the ITIM tyrosine residues at positions 663 and 686 enables PECAM-1 to mediate inhibitory functions by recruiting and activating SHP-2.[7] Our chemical shift perturbation analysis of the PECAM-1 cytoplasmic domain revealed that Y_{686} lay within a region that interacted with lipid, whereas Y_{663} did not. We therefore sought to determine whether the potential for these 2 tyrosines to interact with lipid correlated with their susceptibility to phosphorylation. Members of the Src, Csk, and Fer families of tyrosine kinases are able to phosphorylate PECAM-1.[7,27] Although the tyrosine residues that are predominantly phosphorylated within the human PECAM-1 cytoplasmic domain are Y_{663} and Y_{686},[28] low levels of phosphorylation on Y_{701} have been reported in some cells,[29,30] and Y_{636} can be phosphorylated by Src family kinases in vitro (C.P., unpublished observations). Therefore, we assessed the extent of Y_{663} and Y_{686} phosphorylation in a mutant form of $PECAM_{594-711}$ in which the tyrosine residues at positions 636 and 701 were changed to phenylalanine ($PECAM_{594-711}Y_{636,701}F$). As shown in Figure 3A, phosphorylation of $PECAM_{594-711}Y_{636,701}F$ by the Src family kinases, Src or Fyn, or by the Fps/Fes family kinase Fer, resulted in generation of 2 phosphorylated species (bands 1 and 2), which migrated at slightly higher apparent molecular weights relative to unphosphorylated $PECAM_{594-711}Y_{636,701}F$ on SDS-PAGE. These species were purified to homogeneity by use of Mono Q ion exchange chromatography, which yielded unphosphorylated $PECAM_{594-711}Y_{636,701}F$ and 2 species (peak 1 and peak 2) of phosphorylated $PECAM_{594-711}Y_{636,701}F$ (Figure 3B). Each of these species was subjected to limited digestion with trypsin, and tryptic digests were subjected to mass spectrometric analysis. Results of these studies (Figure 4; Table 2) revealed that tryptic fragments that lack tyrosine residues (peptides A and E) had masses consistent with absence of phosphate groups whether they were generated from unphosphorylated $PECAM_{594-711}Y_{636,701}F$ (Figure 4A; "UN"

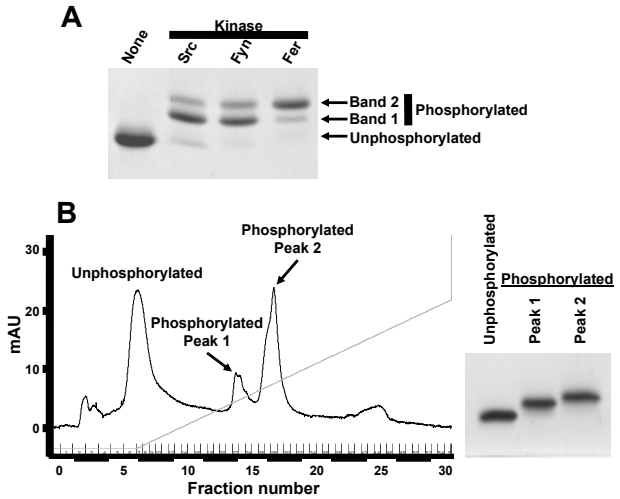

Figure 3. Purification of unphosphorylated and phosphorylated recombinant PECAM-1 cytoplasmic domain species for mass spectrometric analysis. The vector encoding $PECAM_{cyto}$-FP was modified to change tyrosine residues at positions 636 and 701 of the PECAM-1 cytoplasmic domain to phenylalanine ($PECAM_{594-711}Y_{636,701}F$) and used to transform *Escherichia coli.* Protein expression was induced with IPTG, and $PECAM_{594-711}Y_{636,701}F$ was purified as described in supplemental Figure 1. (A) Purified $PECAM_{594-711}Y_{636,701}F$ was left unphosphorylated or subjected to in vitro phosphorylation by Src, Fyn, or Fer tyrosine kinase. Unphosphorylated and phosphorylated $PECAM_{594-711}Y_{636,701}F$ were separated by SDS-PAGE and stained with Coomassie blue. Note that phosphorylated $PECAM_{594-711}Y_{636,701}F$ migrated as 2 species with slightly higher apparent molecular weights than unphosphorylated $PECAM_{594-711}Y_{636,701}F$ on SDS-PAGE. (B) (Left) Unphosphorylated and Fer kinase-phosphorylated $PECAM_{594-711}Y_{636,701}F$ were subjected to ion exchange chromatography to enable purification of unphosphorylated $PECAM_{594-711}Y_{636,701}F$ and separation of the 2 species of phosphorylated $PECAM_{594-711}Y_{636,701}F$ (peak 1 and peak 2) from one another. (Right) Coomassie-stained SDS-PAGE gel showing the purity of unphosphorylated and phosphorylated peaks 1 and 2 of $PECAM_{594-711}Y_{636,701}F$. mAU indicates milliabsorbence units.

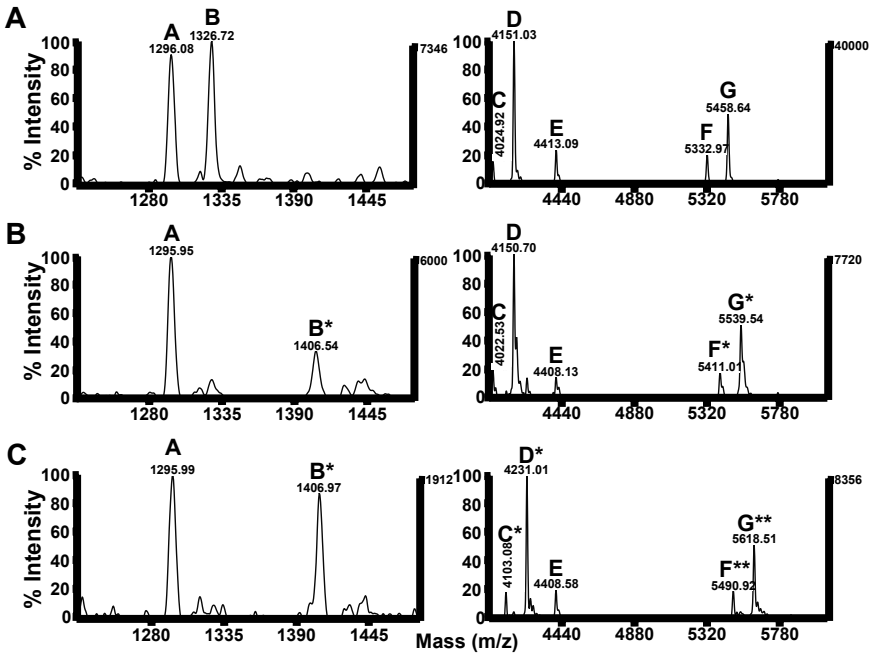

Figure 4. Phosphorylation of the C-terminal PECAM-1 ITIM tyrosine residue (Y_{686}) is required for and is independent of phosphorylation of the N-terminal PECAM-1 ITIM tyrosine residue (Y_{663}). MALDI-TOF mass spectra of tryptic peptides from (A) unphosphorylated, (B) phosphorylated peak 1, or (C) phosphorylated peak 2 species of PECAM$_{594\text{-}711}$Y$_{636,701}$F. Peptides A and E contain no tyrosine (Y) residues, peptide B contains only Y_{686}, peptides C and D contain only Y_{663}, and peptides F and G contain both Y_{663} and Y_{686} (refer to Table 2 for a complete description of the amino acid sequence and location of peptides A-G within full-length PECAM-1). Peptides denoted by a single asterisk (*) represent addition of a single phosphate, whereas those denoted by 2 asterisks (**) contain 2 phosphate moieties. Note that peptides generated from phosphorylated peak 1 include unphosphorylated species that contain either no Y residues (peptides A and E) or only Y_{663} (peptides C and D) and singly phosphorylated species that contain Y_{686} (peptides B*, F*, and G*). Fragments generated from phosphorylated peak 2 include unphosphorylated species that contain no Y residues (peptides A and E), singly phosphorylated species that contain either Y_{686} (peptide B*) or Y_{663} (peptides C* and D*), and doubly phosphorylated species that contain both Y_{686} and Y_{663} (peptides F** and G**). m/z indicates mass-to-charge ratio.

in Table 2) or from either peak 1 (Figure 4B; "Peak 1" in Table 2) or peak 2 (Figure 4C; "Peak 2" in Table 2) species of phosphorylated PECAM$_{594\text{-}711}$Y$_{636,701}$F. Tryptic fragments that contain both Y_{663} and Y_{686} (peptides F and G) had masses consistent with absence of phosphate groups when derived from unphosphorylated PECAM$_{594\text{-}711}$Y$_{636,701}$F (Figure 4A; "UN" in Table 2), addition of 1 phosphate group when derived from peak 1 of phosphorylated PECAM$_{594\text{-}711}$Y$_{636,701}$F (Figure 4B, "Peak 1" in Table 2), and addition of 2 phosphate groups when derived from peak 2 of phosphorylated PECAM$_{594\text{-}711}$Y$_{636,701}$F (Figure 4C; "Peak 2" in Table 2). These results demonstrate that peak 1 corresponds to a monophosphorylated species, whereas peak 2 corresponds to a diphosphorylated species of PECAM$_{594\text{-}711}$Y$_{636,701}$F. The tryptic fragment that contained only Y_{686} (peptide B) had a mass consistent with addition of a phosphate group when derived from either the monophosphorylated (Figure 4B; "Peak 1" in Table 2) or the diphosphorylated (Figure 4C; "Peak 2" in Table 2) species of PECAM$_{594\text{-}711}$Y$_{636,701}$F, which suggests that Y_{686} can be phosphorylated independently of phosphorylation of Y_{663}. In contrast, tryptic fragments that contained only Y_{663} (peptides C and D) had masses consistent with the addition of a phosphate group when they were derived from the diphosphorylated species of PECAM-1$_{594\text{-}711}$Y$_{636,701}$F (Figure 4C; "Peak 2" in Table 2) but not when derived from the monophosphorylated species of PECAM-1$_{594\text{-}711}$Y$_{636,701}$F (Figure 4B; "Peak 1" in Table 2). These results implicate a sequential mechanism for PECAM-1 ITIM phosphorylation, in which phosphorylation of Y_{663} is dependent on prior phosphorylation of Y_{686}.

Identification of PECAM-1 serine phosphorylation sites

PECAM-1 is both constitutively and inducibly phosphorylated on serine residues[7]; however, the sites of serine phosphorylation within the PECAM-1 cytoplasmic domain are not known. To determine which of the 12 serine residues within the cytoplasmic domain of human PECAM-1 are capable of being phosphorylated, we assessed the extent of ^{32}P incorporation into WT or mutant forms of PECAM-1 that contained either all 12 serine residues (12S), alanine substitutions for all 12 serine residues (12S→A), or alanine substitutions for all but 1 of the 12 individual serine residues (11S→A). PECAM-1 constructs encoded phenylalanine substitutions at positions 663 and 686 ($Y_{663,686}$F) to minimize

Table 2. MALDI-TOF analysis of peptides derived from a limited tryptic digest of Fer-phosphorylated PECAM$_{594\text{-}711}$Y$_{636,701}$F

Peptide	PECAM-1 fragment	Potential phospho-tyrosines	Expected monoisotopic masses			Observed monoisotopic masses			Sequence
							Phosphorylated		
			No PO_4	1* PO_4	2** PO_4	UN	Peak 1	Peak 2	
A	644-654	None	1297.6	N/A	N/A	1296.1	1296.0	1296.0	NHAMKPINDNK
B	680(1)-690(1)	Y_{686}	1326.7	1406.6	N/A	1326.7	**1406.5***	**1407.0***	(K)DTETVY$_{686}$SEVR(K)
C	644-679	Y_{663}	4023.0	4102.9	N/A	4024.9	4022.5	**4103.1***	N. . .KEPLNSDVQY$_{663}$TEVQVSSAESHKDLGK
D	644-680	Y_{663}	4151.1	4231.0	N/A	4151.0	4150.8	**4231.0***	N. . .KEPLNSDVQY$_{663}$TEVQVSSAESHKDLGKK
E	605-643 (F636)	None	4408.0	N/A	N/A	4413.1	4408.1	4408.6	AKQMPVEMSRPAVPLLNSNNEKMSDPNMEANSHFGHNDDVR
F	644-690	Y_{663}, Y_{686}	5330.6	5410.6	5490.5	5333.0	**5411.0***	**5490.9****	N. . .KEPLNSDVQY$_{663}$TEVQVSSAESHKDLGKKDTETVY$_{686}$SEVR
G	644-691	Y_{663}, Y_{686}	5458.7	5538.6	5618.6	5458.6	**5539.5***	**5618.5****	N. . .KEPLNSDVQY$_{663}$TEVQVSSAESHKDLGKKDTETVY$_{686}$SEVRK

UN indicates unphosphorylated; and N/A, not applicable.

Bold type denotes peptides containing phosphate groups, with a single asterisk (*) representing addition of a single phospate moiety and 2 asterisks (**) representing addition of 2 phosphate moieties.

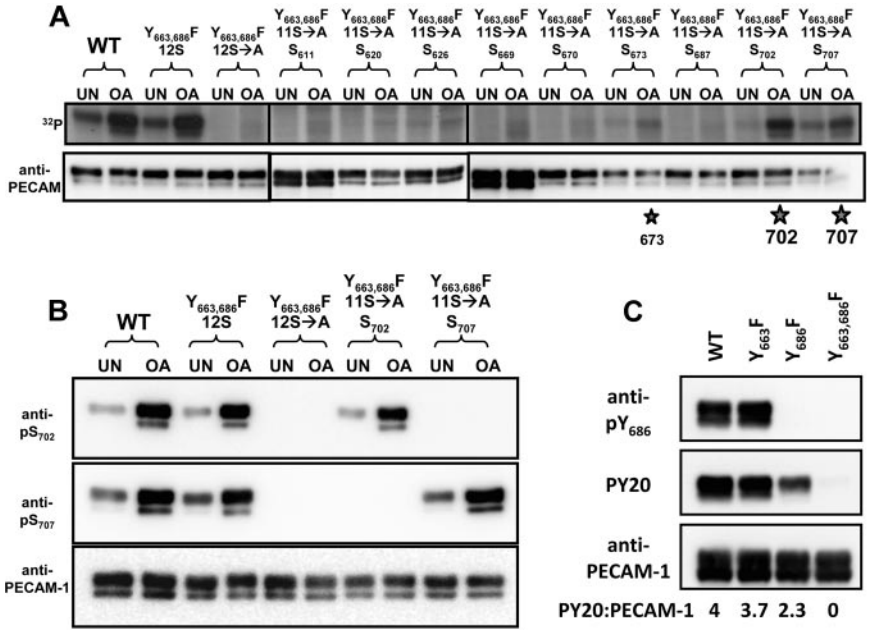

Figure 5. Identification of PECAM-1 serine phosphorylation sites and characterization of phosphoserine-specific antibodies. (A) Identification of S_{702} and S_{707} as major sites of PECAM-1 serine phosphorylation. Levels of incorporation of radiolabeled phosphate (^{32}P) into PECAM-1 immunoprecipitated from untreated (UN) or OA-treated HEK cells expressing WT or mutant forms of human PECAM-1. Mutant forms of PECAM-1 included $Y_{663,686}F(12S)$, in which tyrosine residues at positions 663 and 686 were substituted with phenylalanine; $Y_{663,686}F(12S{\rightarrow}A)$, which contained the tyrosine-to-phenylalanine substitutions, as well as substitution of alanine for all 12 serine residues; and $Y_{663,686}F(11S{\rightarrow}A)$, which contained the tyrosine-to-phenylalanine substitutions at positions 663 and 686, as well as serine-to-alanine substitutions at all but 1 position. At 5 of these positions (620, 670, 687, 702, and 707), serine was found in all of the species in which PECAM-1 had thus far been sequenced, and at 4 of these positions (611, 626, 669, and 673), serine was less well conserved (D.K.N., unpublished observations). Note that the WT and $Y_{663,686}F(12S)$, but not $Y_{663,686}F(12S{\rightarrow}A)$, forms of PECAM-1 were phosphorylated in both untreated and OA-treated HEK 293T cells. Reintroduction of single serine residues revealed preferential serine phosphorylation of PECAM-1 at positions $702 > 707 \gg 673$ (⋆). (B) Characterization of PECAM-1 pS_{702}- and pS_{707}-specific polyclonal antibodies. Western blot analysis of PECAM-1 immunoprecipitates from HEK 293T transfectants described in panel A revealed that affinity-purified rabbit polyclonal anti-pS_{702} (top) and anti-pS_{707} (middle) IgGs both recognized WT and Y663,686F(12S) but not Y663,686F(12S→A) forms of PECAM-1. Reintroduction of a single serine residue at position 702 restored recognition of PECAM-1 by the pS_{702}-specific but not the pS_{707}-specific IgG. Similarly, reintroduction of a single serine residue at position 707 restored recognition of PECAM-1 by the pS_{707}-specific but not the pS_{702}-specific IgG. The presence of PECAM-1 in all PECAM-1 immunoprecipitates was confirmed by binding of a phosphorylation-independent PECAM-1-specific antibody (bottom). (C) Characterization of the PECAM-1 pY_{686}-specific polyclonal antibody. Western blot of PECAM-1 immunoprecipitates from HEK 293T cells transfected with WT, $Y_{663}F$, $Y_{686}F$, or $Y_{663,686}F$ mutant forms of PECAM-1 revealed that rabbit polyclonal anti-pY_{686} (top) recognized WT and $Y_{663}F$ but not $Y_{686}F$ or $Y_{663,686}F$ forms of PECAM-1. Tyrosine phosphorylation of WT, $Y_{663}F$, and $Y_{686}F$ but not $Y_{663,686}F$ forms of PECAM-1 was confirmed by Western blot analysis with pY20 (middle). The presence of PECAM-1 in all PECAM-1 immunoprecipitates was confirmed by binding of a phosphorylation-independent PECAM-1–specific antibody (bottom).

potential incorporation of ^{32}P into tyrosine residues, and transfectants were cultured with the serine/threonine phosphatase inhibitor, OA, to maximize incorporation of ^{32}P into serine residues. As shown in Figure 5A, both untreated and OA-treated cells incorporated high levels of ^{32}P into WT and $Y_{663,686}F(12S)$, but not $Y_{663,686}F(12S{\rightarrow}A)$, forms of PECAM-1. Among the 12 potential sites for serine phosphorylation, PECAM-1 became highly phosphorylated on S_{702} and S_{707}, with weak phosphorylation on S_{673}.

To examine the conditions under which PECAM-1 becomes phosphorylated at its major serine and tyrosine phosphorylation sites, antibodies specific for phosphoserine residues at positions 702 and 707 (anti-pS_{702} and anti-pS_{707}, respectively), as well as an antibody specific for a phosphotyrosine at position 686 (anti-pY_{686}), within PECAM-1 were developed. To verify the specificity of the antibodies, WT and mutant forms of human PECAM-1 were immunoprecipitated from lysates of transiently transfected HEK 293T cells with the human PECAM-1-specific monoclonal antibody PECAM-1.3, separated by SDS-PAGE, and analyzed by Western blot analysis with anti-pS_{702}, anti-pS_{707}, and anti-pY_{686}. As shown in Figure 5B, recognition of PECAM-1 by anti-pS_{702} and anti-pS_{707} depended on the presence of a serine residue at position 702 or 707, respectively, and both reactivities were enhanced by (but did not require) treatment of HEK 293T cell transfectants with OA. Similarly, recognition of PECAM-1 by anti-pY_{686} required the presence of a tyrosine residue at position 686 and coincided with PECAM-1 tyrosine phosphorylation, as measured by Western blot analysis with the phosphotyrosine-specific antibody PY20 (Figure 5C). The finding that PY20 recognized the $Y_{663}F$ form of PECAM-1 better than the $Y_{686}F$ form is consistent with a sequential mechanism for PECAM-1 ITIM phosphorylation, in which Y_{686} is phosphorylated more readily than Y_{663} and Y_{663} is phosphorylated only poorly in the absence of Y_{686}. Treatment of PECAM-1 immunoprecipitates with alkaline phosphatase to dephosphorylate both serine and tyrosine residues abrogated recognition of PECAM-1 by anti-pS_{702}, anti-pS_{707}, and anti-pY_{686} (data not shown). Together, these results demonstrate that antibodies raised against pS_{702}-, pS_{707}-, and pY_{686}-containing PECAM-1 peptides are both sequence specific and phosphorylation dependent.

Characterization of constitutive and inducible serine and tyrosine phosphorylation sites in PECAM-1

Our chemical shift perturbation analysis of the PECAM-1 cytoplasmic domain revealed that S_{702} is contained within a region of the PECAM-1 cytoplasmic domain that interacts with lipid, whereas S_{707} is not. Furthermore, localization of Y_{686} within the segment of the PECAM-1 cytoplasmic domain that interacts with lipid correlates with its preferential phosphorylation relative to Y_{663}, which is located within a region of the PECAM-1 cytoplasmic domain that does not interact with lipid. We therefore sought to determine

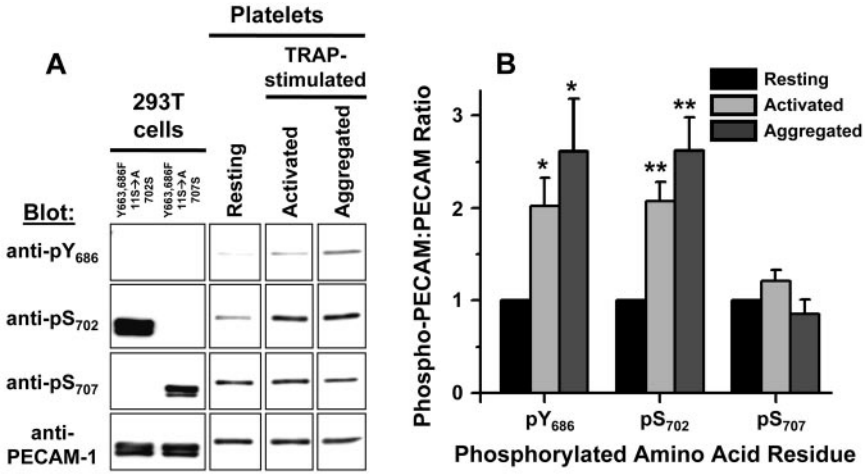

Figure 6. PECAM-1 Y_{686} and S_{702} are inducibly phosphorylated, whereas Y_{707} is constitutively phosphorylated, in human platelets. (A) Left 2 lanes: Western blot analysis of PECAM-1 immunoprecipitates from HEK 293T transfectants expressing Y663,686F(11S→A)702S or Y663,686F(11S→A)707S forms of PECAM-1, which cannot be recognized by the pY_{686}-specific antibody because of the $Y_{686}F$ substitution, demonstrated that recognition of PECAM-1 by pS_{702}- and pS_{707}-specific antibodies depended on the presence of a serine residue at position 702 or 707, respectively. The presence of PECAM-1 in all PECAM-1 immunoprecipitates was confirmed by binding of a phosphorylation-independent PECAM-1–specific antibody. Right 3 lanes: Representative Western blots illustrate stronger binding of pY_{686}- and pS_{702}-specific antibodies to PECAM-1 immunoprecipitated from thrombin receptor activating peptide (TRAP)–activated or TRAP-aggregated platelets relative to resting platelets. In contrast, pY_{707}-specific antibodies bound equally well to PECAM-1 immunoprecipitated from resting or TRAP-activated or TRAP-aggregated platelets. Immunoprecipitation of equal amounts of PECAM-1 from resting or TRAP-activated or TRAP-aggregated platelets was confirmed by binding of a phosphorylation-independent PECAM-1–specific antibody. (B) Quantitative analysis of PECAM-1 pY_{686}, pS_{702}, and pS_{707} levels in resting, TRAP-activated, and TRAP-aggregated human platelets. Western blot band intensities were determined by densitometric analysis, and the ratios of phosphorylated PECAM-1 to total PECAM-1 were calculated. For each antibody, ratios were normalized to values observed in resting platelets. The means ± SEM calculated from 3 independent experiments are shown. $^*P < .05$, $^{**}P < .01$ relative to resting platelets.

whether differences in S_{702} and S_{707} lipid interactions correlate with differences in their susceptibility to phosphorylation. To address this issue, we immunoprecipitated PECAM-1 from lysates of resting, activated, and aggregated platelets. PECAM-1 immunoprecipitates were resolved by SDS-PAGE and subjected to Western blot analysis with anti-pY_{686}, anti-pS_{702}, and anti-pS_{707} antibodies. As shown in Figure 6, PECAM-1 immunoprecipitates from resting, activated, and aggregated platelets contained equal amounts of PECAM-1, which was recognized equally well by anti-pS_{707} under all conditions. In contrast, both anti-pY_{686} and anti-pY_{702} exhibited enhanced recognition of PECAM-1 isolated from activated or aggregated platelets relative to resting platelets. These results demonstrate that PECAM-1 phosphorylation at positions Y_{686} and S_{702} is inducible, whereas phosphorylation at position S_{707} is constitutive, in human platelets.

Proposal and testing of a model for regulation of sequential PECAM-1 phosphorylation by structure-inducing interactions with plasma membrane phospholipids

Our studies revealed that a short segment of the PECAM-1 cytoplasmic domain, encompassing residues 682-702, underwent interactions with plasma membrane-mimetic detergent micelles that promoted adoption of localized α-helical structure (shown schematically in Figure 7A). The membrane-interacting segment contains both a serine (S_{702}) and a tyrosine (Y_{686}) residue that were inducibly and sequentially phosphorylated. Collectively, these findings suggest a model in which ordered phosphorylation and plasma membrane dissociation events coordinate sequential phosphorylation of the PECAM-1 cytoplasmic domain (Figure 7B). Thus, in resting cells, residues near the C-terminus of the PECAM-1 cytoplasmic domain engage in structure-inducing membrane interactions that interfere with its phosphorylation (Figure 7Bi). On cellular activation, phosphorylation of S_{702} alters the overall affinity of the lipid-associating region for the plasma membrane by reducing the local net positive charge at the C-terminal end of the helix (Figure 7Bii). Subsequent dissociation of the PECAM-1 cytoplasmic domain from the plasma membrane renders Y_{686} accessible for phosphorylation, which then enables subsequent phosphorylation at Y_{663} (Figure 7Biii).

To test this model, we used CD spectroscopy to evaluate the conformation of a peptide that contained the membrane-interacting region of the PECAM-1 cytoplasmic domain (PECAM-$1_{684\text{-}711}$) in the presence of lipid vesicles that mimicked the composition of the inner face of the plasma membrane and to determine the effect of phosphorylation of S_{702} and Y_{686} on conformation-inducing plasma membrane interactions (Figure 8). As shown in Figure 8A, vesicles that contained increasing amounts of the anionic phospholipid DMPS, but not those that contained 100% of the zwitterionic phospholipid DMPC, induced changes in PECAM-$1_{684\text{-}711}$ that were consistent with loss of random coil and gain of α-helical content. This effect was most evident in the ~210- to 230-nm range of the PECAM-$1_{684\text{-}711}$ CD spectrum, which exhibited a shallower minimum at 222 nm and acquisition of a new maximum at ~215 nm in the presence of DMPS-containing vesicles. Importantly, the effects of DMPS-containing vesicles on the shape of the PECAM-$1_{684\text{-}711}$ CD spectrum (Figure 8B) and the minimum observed at 222 nm (Figure 8C) were diminished by the presence of pS_{702} and abolished by the presence of both pS_{702} and pY_{686} in the peptide sequence. These results verify the conclusions that residues within the C-terminal segment of the PECAM-1 cytoplasmic domain adopt α-helical conformation in the presence of negatively charged phospholipids and that phosphorylation of serine and tyrosine residues within this segment induces loss of secondary structure, and they support our proposed model for ordered phosphorylation and plasma membrane dissociation events that coordinate sequential phosphorylation of the PECAM-1 cytoplasmic domain.

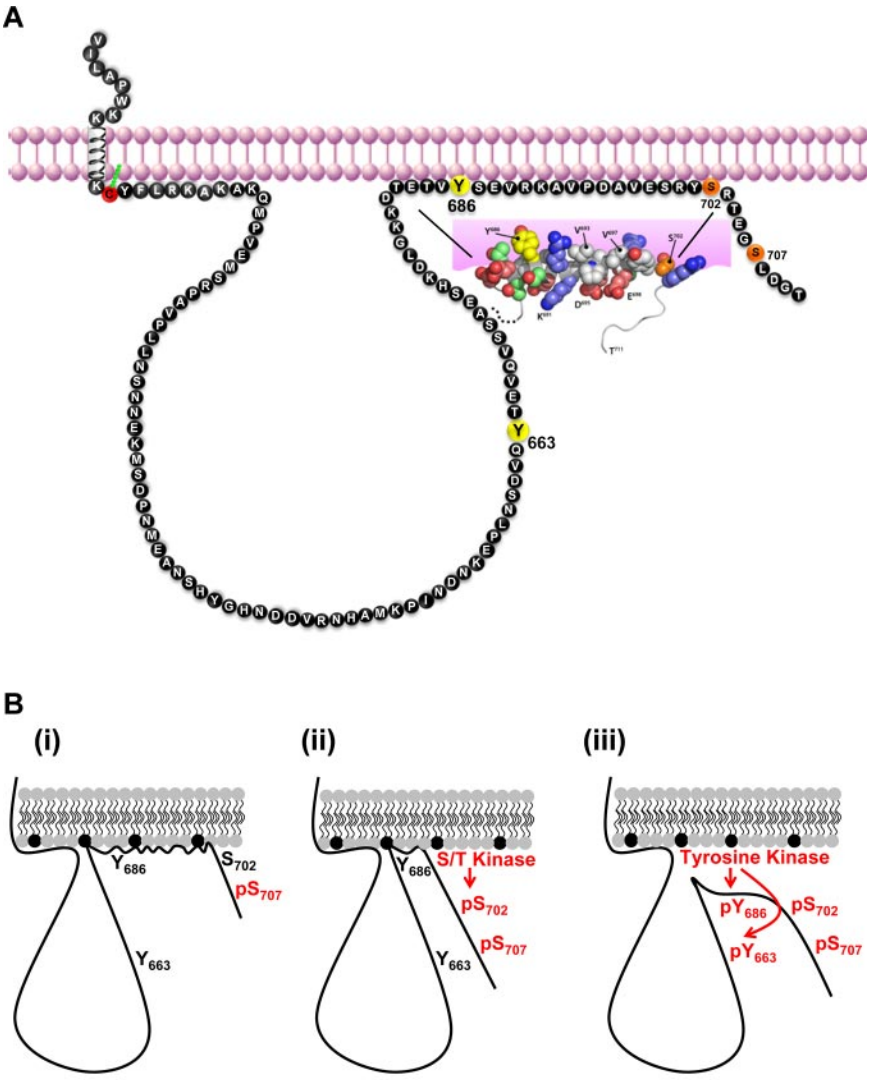

Figure 7. Hypothetical model for regulation of PECAM-1 tyrosine phosphorylation and inhibitory function by PECAM-1 cytoplasmic domain interactions with the plasma membrane. (A) Schematic diagram representing membrane proximity of amino acids within the human PECAM-1 cytoplasmic domain. Amino acids are identified with the single-letter code, and numbering is based on the sequence of the mature human protein. ITIM tyrosine residues are shown in yellow, and the serine residues that are susceptible to inducible (S_{702}) and constitutive (S_{707}) phosphorylation in platelets are shown in orange. The juxtamembrane cytoplasmic cysteine residue that is susceptible to palmitoylation is shown in red. A segment of the PECAM-1 cytoplasmic domain that spans amino acid residues T_{682}-S_{702} forms an amphipathic helix that participates in plasma membrane interactions. Important features of the membrane-interacting segment are that it (1) is bordered by the inducibly phosphorylated serine residue (S_{702}), (2) encompasses the C-terminal ITIM tyrosine residue (Y_{686}), and (3) excludes the N-terminal tyrosine residue (Y_{663}). (B) Model for regulation of PECAM-1 cytoplasmic domain phosphorylation by reversible plasma membrane association. (i) In resting platelets, the PECAM-1 cytoplasmic domain, which is constitutively phosphorylated on S_{707}, binds to the plasma membrane via interactions between hydrophobic amino acids and neutral phospholipids (gray) and between positively charged amino acids and negatively charged phospholipids (black). (ii) Activation of a serine/threonine (S/T) kinase in activated platelets results in phosphorylation of S_{702}, which initiates dissociation of the membrane-interacting segment from the plasma membrane and exposes the C-terminal ITIM tyrosine residue (Y_{686}). (iii) Activation of a tyrosine kinase in aggregated platelets results in phosphorylation of Y_{686}, which enables subsequent phosphorylation of the N-terminal ITIM tyrosine residue (Y_{663}). Phosphorylation of both ITIMs supports SHP-2 binding and PECAM-1 inhibitory function.

Discussion

A central dogma of structural biology is that protein function requires adoption of a particular 3D structure; however, it has recently become apparent that certain classes of functional proteins contain extensive regions of disorder.[31] The family of intrinsically disordered proteins includes signal transducing molecules, which are susceptible to posttranslational modification in the disordered state but are capable, in certain environments, of undergoing a disorder-to-order transition that interferes with posttranslational modification.[32,33] The presence of lipids or lipidlike moieties that mimic the inner face of the plasma membrane is one environment that has been found to both induce secondary structure in and inhibit posttranslational modification of intrinsically unstructured proteins. The best examples of the effects of a lipidlike environment on protein structure and phosphorylation are ITAM-containing sequences within the cytoplasmic domains of TCR-ζ and CD3ϵ signaling subunits, which are unstructured in an aqueous environment but adopt an α-helical conformation in the presence of plasma membrane mimetics that interferes with their phosphorylation.[2-4,22] In the present study, we used the well-characterized dual-ITIM–containing inhibitory receptor family member PECAM-1[7] as a model to determine whether plasma membrane interactions similarly regulate signaling by ITIM-containing receptors. We found that the PECAM-1 cytoplasmic domain is intrinsically unstructured in an aqueous environment but that a short segment of it that encompasses the C-terminal ITIM engages in interactions with plasma membrane mimetics that induce adoption of an α-helical conformation (Figures 1-2 and 8; shown schematically in Figure 7). This finding suggests that phosphorylation of the PECAM-1 C-terminal ITIM, like that of TCR-associated ITAM-containing subunits, is constitutively suppressed by plasma membrane interactions in resting cells. Whether adoption of secondary structure is in fact necessary for plasma membrane interactions to control susceptibility of the PECAM-1 C-terminal ITIM to phosphorylation or is simply a function of the composition of the detergent micelles and lipid vesicles that were used for the present studies, as has been suggested for immune receptor ITAMs,[34] remains to be determined.

HSQC spectral analysis in the presence versus absence of DPC micelles revealed that the C-terminal ITIM of PECAM-1 engages in structure-inducing plasma membrane interactions, whereas the N-terminal ITIM of PECAM-1 does not (Figure 1). The reason for the difference in lipid-binding behavior of the 2 PECAM-1 ITIMs is not apparent; however, some interesting possible explanations arise from a comparison of the physicochemical properties of the PECAM-1 ITIMs with those of lipid-interacting and non–lipid-interacting immune receptor ITAMs. It has been proposed that the

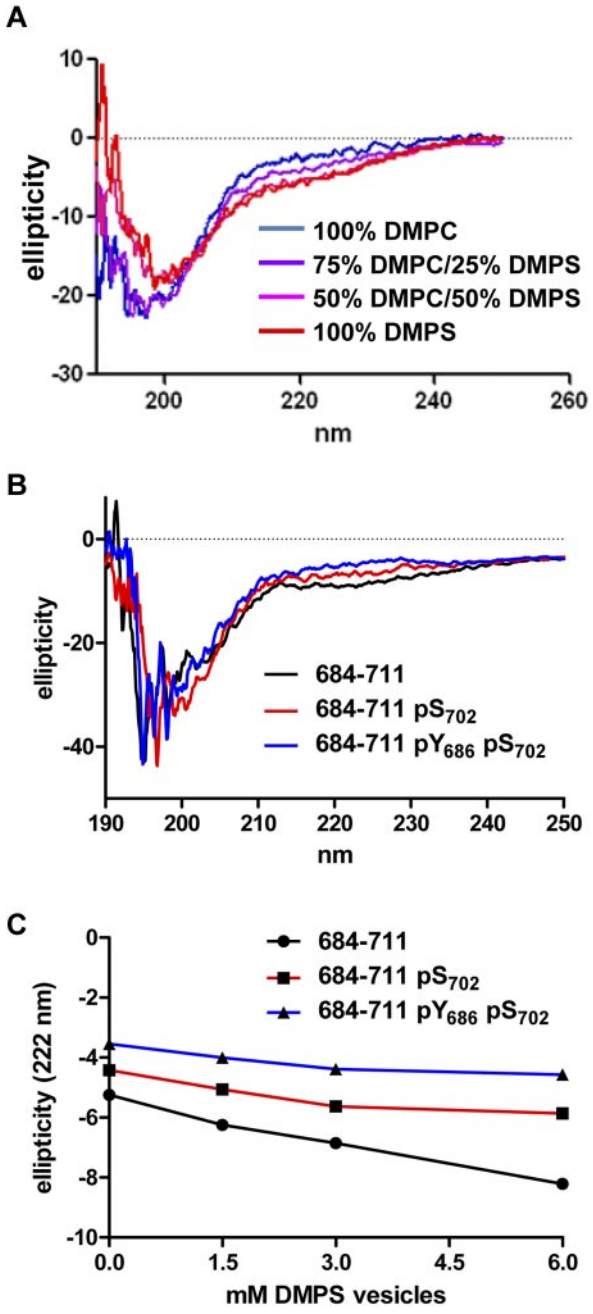

Figure 8. The presence of pS_{702} and pY_{686} within a segment of the PECAM-1 cytoplasmic domain spanning residues 684-711 affects its interaction with anionic phospholipid-containing vesicles. (A) CD spectra of PECAM-$1_{684-711}$ in the presence of lipid vesicles (6mM) that contained 100% DMPC, decreasing amounts of DMPC and increasing amounts of DMPS, or 100% DMPS. Note that PECAM-$1_{684-711}$ exhibited decreased ellipticity at 208 and 222 nm in the presence of vesicles that contained increasing amounts of DMPS relative to vesicles that contained 100% DMPC or buffer alone, which is consistent with increased α-helical content in the presence of anionic phospholipids. (B) CD spectra of PECAM-$1_{684-711}$ peptides that contained no phosphorylated residues (684-711) phosphoserine at position 702 (684-711 pS_{702}), or both phosphoserine at position 702 and phosphotyrosine at position 686 (684-711 pY_{686} pS_{702}) in the presence of vesicles (6mM) that contained 100% DMPS. (C) CD ellipticity measurements at 222 nm of unphosphorylated, pS_{702}-containing, or pY_{686}- and pS_{702}-containing PECAM-$1_{684-711}$ peptides in the presence of increasing concentrations of vesicles (0-6mM) composed of 100% DMPS. Note that the magnitude of the drop in ellipticity at 222 nm was most dramatic with unphosphorylated peptide (slope −0.48), reduced with the peptide that contained pS_{702} (slope −0.23), and almost absent with the peptide that contained both pY_{686} and pS_{702} (slope −0.16). Linear regression analysis revealed that differences between the slopes of the lines were very significant ($P < .01$). These results indicate that the phosphorylated peptides were increasingly insensitive to DMPS-induced α-helix formation.

lipid-binding strength of different ITAMs correlates with protein net charge and with the presence of clustered basic amino acid residues in the region encompassing the ITAM.[35] The present findings support generalization of this model to encompass ITIMs as well. Thus, comparison of the PECAM-1 ITIMs with immune receptor ITAMs (Table 3) reveals that the lipid-interacting portion of the PECAM-1 cytoplasmic domain, which encompasses the C-terminal ITIM, is similar to lipid-interacting ITAMs in that it has an isoelectric point of approximately 6 or higher and possesses 2 adjacent basic residues in close proximity to the ITIM tyrosine residue, Y_{686}. In contrast, the non–lipid-interacting region of the PECAM-1 cytoplasmic domain, which encompasses the N-terminal ITIM, is similar to non–lipid-interacting ITAMs in that it has an isoelectric point of less than 5 and does not contain a cluster of basic residues near the ITIM tyrosine residue, Y_{663}. The finding that Y_{663}, which like Y_{686} is susceptible to inducible phosphorylation,[28,36] does not engage in plasma membrane interactions suggests that its phosphorylation is not directly regulated by plasma membrane interactions. Instead, Y_{663} was only phosphorylated when Y_{686} had been phosphorylated first (Table 2; Figures 3-4). Thus, Y_{686} phosphorylation, which is itself regulated by plasma membrane interactions, may be the event that regulates phosphorylation of Y_{663} and, ultimately, initiation of PECAM-1–mediated inhibitory signaling. The mechanisms involved in sequential phosphorylation of the PECAM-1 ITIMs are not known and are the subject of continuing investigation in our laboratory.

It has long been known that PECAM-1 is susceptible to both constitutive and inducible phosphorylation on serine residues.[37,38] However, neither the sites within PECAM-1 that serve as targets for serine phosphorylation nor the functional relevance of this posttranslational modification have been established. The present study is the first to definitively identify S_{702} and S_{707} as the major sites of serine phosphorylation within PECAM-1 and to demonstrate that PECAM-1 is constitutively phosphorylated on S_{707}, whereas phosphorylation of S_{702} is inducible (Figures 5-6). Previous studies have reported that PECAM-1 serine phosphorylation affects its ability to associate with the cytoskeleton in platelets[37] and endothelial cells,[39] albeit positively in the former and negatively in the latter; however, to the extent that they have been studied, PECAM-1 cytoskeletal interactions do not appear to require either S_{702} or S_{707}.[40] We propose a new role for PECAM-1 serine phosphorylation in regulating its tyrosine phosphorylation. This proposal is predicated on the fact that the inner face of the plasma membrane is enriched in negatively charged phospholipids, including phosphatidylserine and phosphatidylinositol. Electrostatic interactions that involve phosphatidylserine and phosphatidylinositol contribute significantly to membrane binding of several proteins that interact with the inner face of the plasma membrane, including dynamin I, the myristoylated alanine-rich protein kinase C substrate (MARCKS), and numerous members of the Ras, Rho, Arf, and Rab subfamilies of small guanosine triphosphatases (GTPases).[41-44] Such electrostatic interactions rely heavily on association of polybasic clusters of positively charged lysine (K) and arginine (R) residues with negatively charged phospholipids. Interestingly, phosphorylation of serine residues in the vicinity of the polybasic regions has been found to disrupt the electrostatic interactions on which membrane interactions depend and to induce dissociation of these molecules from the membrane, with subsequent redistribution to the cytosol.[41-43] We propose that serine phosphorylation plays a similar role in inducing plasma membrane dissociation of the PECAM-1 cytoplasmic domain so as to enable its tyrosine phosphorylation. Previous studies have demonstrated that inducible PECAM-1 serine phosphorylation precedes

Table 3. Comparison of the physicochemical and lipid-binding properties of lipid-interacting and non–lipid-interacting ITAMs and ITIMs

Signaling molecule	ITIM/ITAM	Sequence	Lipid interaction	pI*	Proximal basic pair†
CD3ϵ	ITAM	PNPD**Y**EPIRKGQRDL**Y**SGLNQRR	Yes	9.7	Yes
TCRζ	ITAM 1	QNQL**Y**NELNLGRREE**Y**DVLDKRR	Yes	6.3	Yes
PECAM-1	C-terminal ITIM	TETV**Y**SEVRKAVPDAVESRYSRT	Yes	5.9	Yes
TCRζ	ITAM 3	HDGL**Y**QGLSTATKDT**Y**DALHMQA	No	5.1	No
PECAM-1	N-terminal ITIM	SDVQ**Y**TEVQVSSAESHKDLGKKD	No	4.8	No
TCRζ	ITAM 2	QEGL**Y**NELQKDKMAEA**Y**SEIGMK	No	4.6	No
CD3δ	ITAM	NDQV**Y**QPLRDRDDAQ**Y**SHLGGNW	No	4.6	No
CD3γ	ITAM	NDQL**Y**QPLKDREDDQ**Y**SHLQGNQ	No	4.4	No
BCR Igβ	ITAM	EDHT**Y**EGLDIDQTAT**Y**EDIVTLR	No	3.9	No
BCR Igα	ITAM	DENL**Y**EGLNLDDCSM**Y**EDISRGL	No	3.6	No

Properties of ITAM sequences were modified from Sigalov et al.[35]

ITAM and ITIM tyrosine (Y) residues are highlighted in bold. The basic amino acid residues, arginine (R) and lysine (K), are underlined.

*Isoelectric points (pI) were calculated with the Compute pI/MW tool using the Swiss Institute of Bioinformatics ExPASy Proteomics Server (http://expasy.org/tools/pi_tool.html).

†Proximal basic pair is defined as 2 adjacent basic amino acid residues either between the 2 ITAM tyrosine residues or within 5 residues of an ITIM tyrosine residue. Note that the sequence between the 2 ITAM tyrosine residues in TCRζ ITAM 2, CD3δ, and CD3γ contains 2 basic amino acid residues but that they are separated by an acidic aspartic acid (D) residue.

its tyrosine phosphorylation in platelets,[36] and in the present study, we have identified S_{702} as the site at which PECAM-1 is inducibly serine phosphorylated. Results of the structural studies reported herein demonstrate that S_{702} is located at the extreme C-terminal end of the membrane-interacting portion of the PECAM-1 cytoplasmic domain and that phosphorylation of S_{702} alters the ability of this segment to adopt secondary structure in the presence of plasma membrane mimetics (Figures 1-2 and 8). Thus, we propose that S_{702} phosphorylation is predicted to reduce the local net positive charge of the membrane-interacting portion of the PECAM-1 cytoplasmic domain and therefore its overall affinity for the plasma membrane. Subsequent dissociation of the PECAM-1 cytoplasmic domain from the plasma membrane would render the C-terminal ITIM accessible for phosphorylation, which would then enable subsequent phosphorylation of the N-terminal ITIM (shown schematically in Figure 7). The extent to which phosphorylation of PECAM-1 on S_{702} affects phosphorylation of the PECAM-1 ITIMs and ITIM-dependent inhibitory function is an important area of future investigation.

Acknowledgments

We thank Robert Arthur for assistance with characterization of phosphoserine- and phosphotyrosine-specific antibodies.

This work was supported by award numbers R01 HL90883 (D.K.N.), U54 GM074901 (B.F.V.), and R01 HL40926 (P.J.N.) from the National Institutes of Health.

Authorship

Contribution: C.P. performed research, collected data, analyzed and interpreted data, and wrote the manuscript; B.L.L. performed research, analyzed and interpreted data, and wrote the manuscript; F.C.P. performed research and collected data; T.H. performed research, collected data, analyzed and interpreted data, and wrote the manuscript; P.J.N. designed research, analyzed and interpreted data, and wrote the manuscript; B.F.V. designed research, analyzed and interpreted data, and wrote the manuscript; and D.K.N. designed research, analyzed and interpreted data, and wrote the manuscript.

Conflict-of-interest disclosure: The authors declare no competing financial interests.

Correspondence: Debra K. Newman, PhD, Blood Research Institute, 8727 Watertown Plank Rd, Milwaukee, WI 53226; e-mail: debra.newman@bcw.edu.

References

1. Daeron M, Jaeger S, Du PL, Vivier E. Immunoreceptor tyrosine-based inhibition motifs: a quest in the past and future. *Immunol Rev*. 2008;224(1):11-43.
2. Aivazian D, Stern LJ. Phosphorylation of T cell receptor zeta is regulated by a lipid dependent folding transition. *Nat Struct Biol*. 2000;7(11):1023-1026.
3. Duchardt E, Sigalov AB, Aivazian D, Stern LJ, Schwalbe H. Structure induction of the T-cell receptor zeta-chain upon lipid binding investigated by NMR spectroscopy. *Chembiochem*. 2007;8(7):820-827.
4. Xu C, Gagnon E, Call ME, et al. Regulation of T cell receptor activation by dynamic membrane binding of the CD3epsilon cytoplasmic tyrosine-based motif. *Cell*. 2008;135(4):702-713.
5. Newman PJ. Switched at birth: a new family for PECAM-1. *J Clin Invest*. 1999;103(1):5-9.
6. Newman PJ, Berndt MC, Gorski J, et al. PECAM-1 (CD31) cloning and relation to adhesion molecules of the immunoglobulin gene superfamily. *Science*. 1990;247(4947):1219-1222.
7. Newman PJ, Newman DK. Signal transduction pathways mediated by PECAM-1: new roles for an old molecule in platelet and vascular cell biology. *Arterioscler Thromb Vasc Biol*. 2003;23(6):953-964.
8. Farrow NA, Zhang O, Forman-Kay JD, Kay LE. A heteronuclear correlation experiment for simultaneous determination of 15N longitudinal decay and chemical exchange rates of systems in slow equilibrium. *J Biomol NMR*. 1994;4(5):727-734.
9. Lytle BL, Peterson FC, Tyler EM, et al. Solution structure of *Arabidopsis thaliana* protein At5g39720.1, a member of the AIG2-like protein family. *Acta Crystallogr Sect F Struct Biol Cryst Commun*. 2006;62(pt 6):490-493.
10. Delaglio F, Grzesiek S, Vuister GW, Zhu G, Pfeifer J, Bax A. NMRPipe: a multidimensional spectral processing system based on UNIX pipes. *J Biomol NMR*. 1995;6(3):277-293.
11. Bahrami A, Assadi AH, Markley JL, Eghbalnia HR. Probabilistic interaction network of evidence algorithm and its application to complete labeling of peak lists from protein NMR spectroscopy. *PLoS Comput Biol*. 2009;5(3):e1000307.
12. Bartels C, Xia T, Billeter M, Guntert P, Wuthrich K. The program XEASY for computer-supported NMR spectral analysis of biological macromolecules. *J Biomol NMR*. 1995;6(1):1-10.
13. Mulder FA, Schipper D, Bott R, Boelens R. Altered flexibility in the substrate-binding site of related native and engineered high-alkaline *Bacillus* subtilisins. *J Mol Biol*. 1999;292(1):111-123.
14. Shen Y, Delaglio F, Cornilescu G, Bax A. TALOS+: a hybrid method for predicting protein backbone torsion angles from NMR chemical shifts. *J Biomol NMR*. 2009;44(4):213-223.
15. Güntert P. Automated NMR structure calculation with CYANA. *Methods Mol Biol*. 2004;278:353-378.
16. Linge JP, Williams MA, Spronk CA, Bonvin AM,

Nilges M. Refinement of protein structures in explicit solvent. *Proteins*. 2003;50(3):496-506.

17. Schwieters CD, Kuszewski JJ, Tjandra N, Clore GM. The Xplor-NIH NMR molecular structure determination package. *J Magn Reson*. 2003;160(1):65-73.
18. Metzler WJ, Constantine KL, Friedrichs MS, et al. Characterization of the three-dimensional solution structure of human profilin: ^{1}H, ^{13}C, and ^{15}N NMR assignments and global folding pattern. *Biochemistry*. 1993;32(50):13818-13829.
19. Schwarzinger S, Kroon GJ, Foss TR, Chung J, Wright PE, Dyson HJ. Sequence-dependent correction of random coil NMR chemical shifts. *J Am Chem Soc*. 2001;123(13):2970-2978.
20. Schwarzinger S, Kroon GJ, Foss TR, Wright PE, Dyson HJ. Random coil chemical shifts in acidic 8 M urea: implementation of random coil shift data in NMRView. *J Biomol NMR*. 2000;18(1):43-48.
21. Dosztanyi Z, Csizmok V, Tompa P, Simon I. The pairwise energy content estimated from amino acid composition discriminates between folded and intrinsically unstructured proteins. *J Mol Biol*. 2005;347(4):827-839.
22. Sigalov A, Aivazian D, Stern L. Homooligomerization of the cytoplasmic domain of the T cell receptor zeta chain and of other proteins containing the immunoreceptor tyrosine-based activation motif. *Biochemistry*. 2004;43(7):2049-2061.
23. Kallick DA, Tessmer MR, Watts CR, Li CY. The use of dodecylphosphocholine micelles in solution NMR. *J Magn Reson B*. 1995;109(1):60-65.
24. Beswick V, Roux M, Navarre C, et al. ^{1}H- and ^{2}H-NMR studies of a fragment of PMP1, a regulatory subunit associated with the yeast plasma membrane H^{+}-ATPase: conformational properties and lipid-peptide interactions. *Biochimie*. 1998;80(5-6):451-459.
25. Hornemann S, von Schroetter C, Damberger FF, Wuthrich K. Prion protein-detergent micelle interactions studied by NMR in solution. *J Biol Chem*. 2009;284(34):22713-22721.
26. Jarvet J, Danielsson J, Damberg P, Oleszczuk M, Graslund A. Positioning of the Alzheimer Abeta(1-40) peptide in SDS micelles using NMR and paramagnetic probes. *J Biomol NMR*. 2007;39(1):63-72.
27. Kogata N, Masuda M, Kamioka Y, et al. Identification of Fer tyrosine kinase localized on microtubules as a platelet endothelial cell adhesion molecule-1 phosphorylating kinase in vascular endothelial cells. *Mol Biol Cell*. 2003;14(9):3553-3564.
28. Jackson DE, Kupcho KR, Newman PJ. Characterization of phosphotyrosine binding motifs in the cytoplasmic domain of platelet/endothelial cell adhesion molecule-1 (PECAM-1) that are required for the cellular association and activation of the protein-tyrosine phosphatase, SHP-2. *J Biol Chem*. 1997;272(40):24868-24875.
29. Ilan N, Cheung L, Miller S, Mohsenin A, Tucker A, Madri JA. PECAM-1 is a modulator of STAT family member phosphorylation and localization: lessons from a transgenic mouse. *Dev Biol*. 2001;232(1):219-232.
30. Udell CM, Samayawardhena LA, Kawakami Y, Kawakami T, Craig AW. Fer and Fps/Fes participate in a Lyn-dependent pathway from FcεRI to platelet-endothelial cell adhesion molecule 1 to limit mast cell activation. *J Biol Chem*. 2006;281(30):20949-20957.
31. Dyson HJ, Wright PE. Intrinsically unstructured proteins and their functions. *Nat Rev Mol Cell Biol*. 2005;6(3):197-208.
32. Dunker AK, Brown CJ, Lawson JD, Iakoucheva LM, Obradovic Z. Intrinsic disorder and protein function. *Biochemistry*. 2002;41(21):6573-6582.
33. Iakoucheva LM, Radivojac P, Brown CJ, et al. The importance of intrinsic disorder for protein phosphorylation. *Nucleic Acids Res*. 2004;32(3):1037-1049.
34. Sigalov AB, Hendricks GM. Membrane binding mode of intrinsically disordered cytoplasmic domains of T cell receptor signaling subunits depends on lipid composition. *Biochem Biophys Res Commun*. 2009;389(2):388-393.
35. Sigalov AB, Aivazian DA, Uversky VN, Stern LJ. Lipid-binding activity of intrinsically unstructured cytoplasmic domains of multichain immune recognition receptor signaling subunits. *Biochemistry*. 2006;45(51):15731-15739.
36. Jackson DE, Ward CM, Wang R, Newman PJ. The protein-tyrosine phosphatase SHP-2 binds PECAM-1 and forms a distinct signaling complex during platelet aggregation: evidence for a mechanistic link between PECAM-1 and integrin-mediated cellular signaling. *J Biol Chem*. 1997;272(11):6986-6993.
37. Newman PJ, Hillery CA, Albrecht R, et al. Activation-dependent changes in human platelet PECAM-1: phosphorylation, cytoskeletal association, and surface membrane redistribution. *J Cell Biol*. 1992;119(1):239-246.
38. Zehnder JL, Hirai K, Shatsky M, McGregor JL, Levitt LJ, Leung LLK. The cell adhesion molecule CD31 is phosphorylated after cell activation: down-regulation of CD31 in activated T lymphocytes. *J Biol Chem*. 1992;267(8):5243-5249.
39. Ilan N, Cheung L, Pinter E, Madri JA. Platelet-endothelial cell adhesion molecule-1 (CD31), a scaffolding molecule for selected catenin family members whose binding is mediated by different tyrosine and serine/threonine phosphorylation. *J Biol Chem*. 2000;275(28):21435-21443.
40. Biswas P, Zhang J, Schoenfeld JD, et al. Identification of the regions of PECAM-1 involved in beta- and gamma-catenin associations. *Biochem Biophys Res Commun*. 2005;329(4):1225-1233.
41. Powell KA, Valova VA, Malladi CS, Jensen ON, Larsen MR, Robinson PJ. Phosphorylation of dynamin I on Ser-795 by protein kinase C blocks its association with phospholipids. *J Biol Chem*. 2000;275(16):11610-11617.
42. Kim J, Shishido T, Jiang X, Aderem A, McLaughlin S. Phosphorylation, high ionic strength, and calmodulin reverse the binding of MARCKS to phospholipid vesicles. *J Biol Chem*. 1994;269(45):28214-28219.
43. Heo WD, Inoue T, Park WS, et al. PI(3,4,5)P3 and PI(4,5)P2 lipids target proteins with polybasic clusters to the plasma membrane. *Science*. 2006;314(5804):1458-1461.
44. Goldenberg NM, Steinberg BE. Surface charge: a key determinant of protein localization and function. *Cancer Res*. 2010;70(4):1277-1280.